Title

The Tail of Kinesin-14a in Giardia Is a Dual Regulator of Motility

Journal

Current Biology, 30(18)

ISSN

0960-9822

Authors

Tseng, Kuo-Fu
Mickolajczyk, Keith J
Feng, Guangxi
et al.

Publication Date

2020-09-01

DOI

10.1016/j.cub.2020.06.090

Peer reviewed

Published in final edited form as:

Curr Biol. 2020 September 21; 30(18): 3664–3671.e4. doi:10.1016/j.cub.2020.06.090.

The tail of kinesin-14a in *Giardia* is a dual regulator of motility

Kuo-Fu Tseng[1,†], **Keith J. Mickolajczyk**[2,3,†], **Guangxi Feng**[1,†], **Qingzhou Feng**[2], **Ethiene S. Kwok**[1], **Jesse Howe**[4], **Elisar J. Barbar**[4], **Scott C. Dawson**[5], **William O. Hancock**[2,3], **Weihong Qiu**[1,4,*]

[1]Department of Physics, Oregon State University, Corvallis, Oregon 97331, USA

[2]Department of Biomedical Engineering, Penn State University, University Park, Pennsylvania 16802, USA

[3]Intercollege Graduate Degree Program in Bioengineering, Penn State University, University Park, Pennsylvania 16802, USA

[4]Department of Biochemistry and Biophysics, Oregon State University, Corvallis, Oregon 97331, USA

[5]Department of Microbiology, UC Davis, Davis, California 95616, USA

SUMMARY

Kinesin-14s are microtubule-based motor proteins that play important roles in mitotic spindle assembly [1]. Ncd-type kinesin-14s are a subset of kinesin-14 motors that exist as homodimers with an N-terminal microtubule-binding tail, a coiled-coil central stalk (central stalk), a neck, and two identical C-terminal motor domains. To date, no Ncd-type kinesin-14 has been found to naturally exhibit long-distance minus-end-directed processive motility on single microtubules as individual homodimers. Here, we show that GiKIN14a from *Giardia intestinalis* [2] is an unconventional Ncd-type kinesin-14 that uses its N-terminal microtubule-binding tail to achieve minus-end-directed processivity on single microtubules over μm distances as a homodimer. We further find that while truncation of the N-terminal tail greatly reduces GiKIN14a processivity, the resulting tailless construct GiKIN14a-Δtail is still a minimally processive motor and moves its center-of-mass via discrete 8-nm steps on the microtubule. In addition, full-length GiKIN14a has significantly higher stepping and ATP hydrolysis rates than does GiKIN14a-Δtail. Inserting a flexible polypeptide linker into the central stalk of full-length GiKIN14a nearly reduces its ATP hydrolysis rate to that of GiKIN14a-Δtail. Collectively, our results reveal that the N-terminal tail of

*Lead Contact and Correspondence: Weihong.Qiu@physics.oregonstate.edu (WQ).
†These authors contributed equally

AUTHOR CONTRIBUTIONS

W.Q. conceived and supervised the study; Q.F. and S.C.D. provided reagents; J.H. and E.J.B. performed circular dichroism measurements; E.S.K. performed the hydrodynamic and analytic gel filtration experiments; K.-F.T., K.J.M., and G.F. performed all other experiments; K.-F.T., K.J.M., G.F., J.H., E.J.B., W.O.H., and W.Q. performed the analysis; all authors participated in interpreting the results; and W.Q. wrote the paper with the input from other authors.

DECLARATION OF INTERESTS

The authors declare no competing interests.

GiKIN14a is a *de facto* dual regulator of motility and reinforce the notion of the central stalk as a key mechanical determinant of kinesin-14 motility [3].

eTOC Blurb

Tseng *et al.* show that the N-terminal tail of kinesin-14a from *Giardia intestinalis* is a dual regulator of motility, enabling the kinesin motor for long-distance minus-end-directed processivity on the microtubule and acting to accelerate the stepping and ATP hydrolysis rates of the motor.

RESULTS

Kinesins are microtubule-based motor proteins that convert chemical energy stored in adenosine triphosphate (ATP) into mechanical work for many essential cellular processes [4,5]. All kinesins contain at least one highly conserved catalytic motor domain that harbors both the ATP-binding site and the microtubule-binding site. The kinesin superfamily can be divided into 14 subfamilies (kinesin-1 through kinesin-14) and an orphan group based on the sequence homology in the motor domains [6]. It is well established that kinesin-14s play important roles in the assembly and maintenance of bipolar mitotic spindles [1]. Unlike kinesins from other subfamilies, which have their motor domains located either near the N-terminus or in the middle, kinesin-14s uniquely have their motor domains located near the C-terminus [7]. Kinesin-14s do not exclusively have the same oligomerization and domain composition: Kar3 from *Saccharomyces cerevisiae* forms a heterodimer with the nonmotor partners Cik1 or Vik1 [8,9]; OsKCH2 from *Oryza sativa* forms a homodimer with an actin-binding calponin-homology domain at the N-terminus [10]; Kif25 and KifC3 from *Homo sapiens* both exist as a homotetramer [11,12]; and the majority of kinesin-14s, including the founding kinesin-14 Ncd from *Drosophila melanogaster* [13,14], KlpA from *Aspergillus nidulans* [15], and KifC1/HSET from *Homo sapiens,* are homodimers with an N-terminal nonmotor microtubule-binding tail, a coiled-coil central stalk (central stalk), and two identical C-terminal motor domains. Hereinafter, these homodimeric kinesin-14 motors with an N- terminal nonmotor microtubule-binding tail are referred to as Ncd-type kinesin-14s.

For over twenty years since the discovery of the first kinesin-14 Ncd, the kinesin-14 subfamily was thought to consist of exclusively minus-end-directed nonprocessive motors that exhibit directional preference for the microtubule minus ends in ensembles but lack the ability to generate processive motility as individual dimeric motors. However, recent studies have revealed three unconventional kinesin-14s — Kar3 [8,9], OsKCH2 [10], and KlpA [16] — that are intrinsically processive and capable of generating long-distance unidirectional motility on single microtubules as individual dimers. Several studies have demonstrated that a number of kinesins from other subfamilies depend on nonmotor microtubule-binding domains to either achieve processive motility [17] or gain enhanced processivity [18–20]. In contrast, despite having an N-terminal microtubule-binding tail, no Ncd-type kinesin-14 motor has been found to naturally generate long-distance minus-end-directed processive motility on single microtubules as individual dimers. It is worth emphasizing that microtubule binding by the N-terminal tail enables the Ncd-type kinesin-14 KlpA to achieve processive motility on single microtubules towards the plus ends instead of the minus ends [16]. Interestingly, our recent work [3] showed that two Ncd-type kinesin-14s — KlpA

(processive and plus-end-directed) and Ncd (nonprocessive and minus-end-directed) — can both be converted into highly processive minus-end-directed motors via insertion of a flexible polypeptide linker in the central stalk. This work prompted us to determine in the present work whether unexplored Ncd-type kinesin-14s may exist that combine a microtubule-binding tail domain and a central stalk with suitable flexibility to naturally achieve long-distance minus-end-directed processive motility as individual homodimers on single microtubules.

GiKIN14a Exhibits Minus-End-Directed Micrometer Processivity on Single Microtubules as Individual Homodimers

GiKIN14a is a kinesin-14 from an ancient eukaryote *Giardia intestinalis* [2], We found that the N-terminal tail of GiKIN14a (Figure 1A) binds to microtubules *in vitro* in an ATP-independent manner (Figures S1A and S1B), and that this interaction is mediated by the negatively charged C-terminal E-hooks of microtubules (Figures S1B and S1C). We further found that GiKIN14a is predicted to contain an internal hinge in its central stalk (Figure 1B), similar to a mutant Ncd (Ncd-3xGS) that we previously engineered to gain processive motility by inserting a flexible polypeptide linker in the central stalk [3]. Notably, such an internal hinge is absent from the predicted coiled-coil profile of the central stalk of wildtype Ncd (Ncd-WT, Figure 1B). To confirm this prediction, we performed circular dichroism spectroscopy to compare the α-helical content of the central stalks of GiKIN14a, Ncd-3xGS and Ncd-WT (Figure 1C). Consistent with the coiled-coil predictions (Figure 1B), the central stalks of GiKIN14a and Ncd-3xGS have similar α-helical contents, which are both less than that of the central stalk of Ncd-WT (Figure 1C). Collectively, the presence of a microtubule-binding tail and a flexible coiled-coil stalk in GiKIN14a led us to hypothesize that GiKIN14a may naturally exhibit processive minus-end-directed motility on single microtubules.

To test this hypothesis, we engineered GFP-GiKIN14a, a recombinant full-length GiKIN14a with an N-terminal GFP (Figure 1A). Like other kinesin-14 motors [10,16,21,22], GFP-GiKIN14a exhibited directional preference for microtubule minus-ends in the ensemble microtubule-gliding assay (Figure 1D). When we performed a single-molecule motility assay to visualize the movement of GFP-GiKIN14a on polarity-marked single microtubules, individual GFP-GiKIN14a molecules were observed to move toward the microtubule minus ends in a processive manner (Figure 1E and Video S1). Quantitative kymograph analyses of GFP-GiKIN14a motility revealed a characteristic run-length of 3.6 ± 0.3 μm (mean ± SE, n = 278, Figure 1F) and a mean velocity of 260 ± 80 nm s^{-1} (mean ± SD, n = 278, Figure 1G). Since clustering of nonprocessive kinesin-14 motors has been shown to result in processive motility on single microtubules [21,23], we performed two different assays — single-molecule photobleaching and hydrodynamic analysis [16] — to determine the oligomerization of GFP-GiKIN14a. The single-molecule photobleaching analysis showed that GFP-GiKIN14a predominantly photobleached in one or two steps (Figure 1H), similar to other dimeric kinesins [16,21]. In agreement with the photobleaching analysis, the hydrodynamic analysis yielded a molecular weight similar to the theoretical value of a GFP-GiKIN14a homodimer (Figure S2A). Thus, we conclude that full-length GiKIN14a is an

Ncd-type kinesin-14 that is capable of generating processive minus-end-directed motility on single microtubules as individual homodimers.

The N-terminal Tail Is a Diffusive Tether Required for GiKIN14a to Achieve Micrometer Processivity

To determine whether GiKIN14a behaves similarly to the *A. nidulans* kinesin-14 KIpA [16] and utilizes its N-terminal microtubule-binding tail to achieve pm-distance processivity, we engineered GFP-GiKIN14a-Δtail that lacks the N-terminal microtubule-binding tail (Figure 2A). Similar to full-length GFP-GiKIN14a, GFP-GiKIN14a-Δtail formed a homodimer in solution (Figures 2B and S2B) and exhibited directional preference for microtubule minus-ends in the microtubule-gliding assay (Figure 2C). However, GFP-GiKIN14a-Δtail lacked the ability of GiKIN14a to generate μm-distance processivity under the same experimental conditions on single microtubules (Figure 2D and Video S2). These results imply that the N-terminal tail of GiKIN14a is required for the motor to achieve processive motility over μm distances on single microtubules.

We next asked whether the N-terminal tail enables full-length GFP-GiKIN14a to achieve μm-distance processivity by directly interacting with the C-terminal motor domains. To address this, we performed analytical size-exclusion chromatography to compare the elution profiles of GFP-GiKIN14a-tail, GFP-GiKIN14a-Δtail, and a mixture of GFP-GiKIN14a-tail and GFP-GiKIN14a-Δtail. The results showed that the elution profiles of GFP-GiKIN14a-tail and GFP-GiKIN14a-Δtail are unaffected by the presence of each other (Figure S1D), suggesting that the N-terminal tail of GiKIN14a does not directly interact with the C-terminal motor domains for processivity enhancement. We also performed single-molecule motility experiments to determine the behavior of GFP-GiKIN14a-tail (Figure 1A) on single microtubules. GFP-GiKIN14a-tail binds to and diffuses on microtubules with a diffusion coefficient of $D = 0.93 \pm 0.05\ \mu m^2\ s^{-1}$ (mean ± SD, N = 277, and Figure S1E), which closely matches the diffusion coefficient measured for the tail domain of CENP-E [18]. Taken together, our results suggest that, instead of directly binding to the C-terminal motor domain, the N-terminal tail of GiKIN14a acts as a diffusive tether to enable the motor to achieve processive motility over μm distances on single microtubules.

GiKIN14a-Δtail Steps on Single Microtubules to Exhibit Submicrometer Processivity

Using high-resolution optical trapping, Reinemann and colleagues [24] recently demonstrated that human kinesin-14 HSET is a minimally processive motor that is capable of taking several consecutive 8-nm steps before dissociating from the microtubule. We thus wanted to determine whether GiKIN14a-Δtail is similarly able to generate processive motility over distances below the measurement capability of our fluorescent single-molecule assays. To address this, we attached a 30-nm gold nanoparticle to the N-terminus of GFP-GiKIN14a-Δtail and tracked its position in the presence of 2 mM ATP with a temporal resolution of 1,000 frames per second using totalinternal reflection dark-field microscopy [25]. Our tracking experiments showed that similar to HSET [24], GFP-GiKIN14a-Δtail exhibited directional motility on single microtubules with a run- length of 0.20 ± 0.02 μm (mean ± SE, n = 63, Figures S3A and S3B). Furthermore, our tracking experiments showed that the center-of-mass of GFP-GiKIN14a-Δtail moved along the microtubule long axis with

discrete steps consisting of consecutive forward steps (minus-end-directed steps, green arrows) and occasional backward steps (red arrows) (Figure 3A). Quantitative analysis revealed a step size histogram with a major peak corresponding to a forward step of ~8.7 nm and a minor peak corresponding to a backward one of ~7.8 nm (Figure 3B).

Clustering of two kinesin dimers has been shown to result in a dominant existence of 4-nm steps [26]. Notably, the step size histogram in Figure 3B clearly lacks an obvious peak at ~4 nm, implying that the stepping behavior of GFP-GiKIN14a-Δtail was not due to the unintended clustering of multiple nonprocessive GiKIN14a-Δtail motors on a single gold nanoparticle. To further rule out the possibility that the observed sub-μm processivity of GiKIN14a-Δtail was due to the unintended clustering of multiple motors on a single gold nanoparticle, we performed two additional control experiments. First, we carried out a landing rate assay, which showed that the number of landing events was proportional to the motor-to-gold molar ratio (Figure S3C), indicative of one GFP-GiKIN14a-Δtail dimer per gold nanoparticle [27]. Second, we generated an artificial tetramer GFP-GiKIN14a-Δtail^{T} (Figures S3A and S3D) by clustering two GFP-GiKIN14a-Δtail dimers through a GCN4 parallel tetramer motif [21] and performed single-molecule motility experiments to visualize its motility on the microtubules. The results showed that GFP-GiKIN14a-Δtail^{T} moved at 90 ± 40 nm s^{-1} (mean ± SD, n = 265) with a characteristic run-length of 2.5 ± 0.1 μm (mean ± SE, n = 265, Figures S3E–S3G and Video S3), more than ten times the run length of GFP-GiKIN14a-Δtail (Figure S3B). Together, these data strongly argue against the notion that the sub-micron processivity of gold nanoparticle-labeled GFP-GiKIN14a-Δtail is due to clustering and demonstrate that GiKIN14a-Δtail is sufficient to exhibit processive motility over sub-μm distances on single microtubules as individual homodimers.

The N-terminal Tail Enhances GiKIN14a Stepping and ATP Hydrolysis

To better understand how its N-terminal tail enhances the processivity of GiKIN14a, we labeled the N-terminus of full-length GFP-GiKIN14a with a gold nanoparticle and tracked its position using the dark-field tracking assay [25]. Similar to the tailless GFP-GiKIN14a-Δtail dimer (Figure 3A), forward steps (green arrows) and apparent backward steps (red arrows) along the microtubule long axis were clearly observed for GFP-GiKIN14a (Figure 3C). In addition, the stepping traces contained occasional large jumps (black arrows, Figure 3C), which were not observed in the stepping traces of GiKIN14a-Δtail (Figure 3A). Consistent with these observations, the step size distribution of full-length GiKIN14a (Figure 3D) was broader than that of GiKIN14a-Δtail (Figure 3B).

We next extracted and analyzed the dwell times (the waiting times between two successive steps) of GFP-GiKIN14a-Δtail and GFP-GiKIN14a from their respective stepping traces (Figure 3E). Both dwell time histograms were well-described by single-exponential distributions. The mean dwell time of GFP-GiKIN14a-Δtail was $\tau^{\Delta tail}$ = 0.070 ± 0.002 s (mean ± SE, N = 834 steps), yielding a stepping rate of $k^{\Delta tail}$ = 14.2 s^{-1} (= $1/\tau^{\Delta tail}$). In contrast, the mean dwell time of GFP-GiKIN14a was τ^{FL} = 0.029 ± 0.001 s (mean ± SE, N = 2618 steps), yielding a considerably faster stepping rate of k^{FL} = 34.5 s^{-1}. The difference between $k^{\Delta tail}$ and k^{FL} suggests that the N-terminal tail of GiKIN14a somehow accelerates the mechanochemical cycle of the C-terminal motor domains. To test this, we measured the

microtubule-stimulated ATPase activities of GFP-GiKIN14a-Δtail and GFP-GiKIN14a in solution. Both ATPase rates were well-described by the Michaelis-Menten model (Figure 3F), and yielded ATP turnover rates of 10.0 ± 0.7 s^{-1} (mean ± SE) and 25.7 ± 1.8 s^{-1} (mean ± SE) for GFP-GiKIN14a-Δtail and GFP-GiKIN14a, respectively.

Based on the difference between full-length GiKIN14a and the tailless GiKIN14a-Δtail in both stepping and ATPase rates, we speculated that there may be mechanochemical communication between the N-terminal tail and the C-terminal motor domains through the central stalk in full-length GiKIN14a. To test this possibility, we engineered GFP-GiKIN14a-3xGS — a full-length mutant containing a flexible polypeptide linker (-GSGSGS-) inserted next to H214 in its central stalk — and measured its microtubule-stimulated ATPase activity. The results showed that weakening head-tail communication by increasing the flexibility of the central stalk reduced the ATP turnover rate to 14.3 ± 0.4 s^{-1} (mean ± SE, Figure 3F), nearly the same as that of the tailless dimer GFP-GiKIN14a-Δtail (Figure 3F).

DISCUSSION

To summarize, we found that GiKIN14a from *G. intestinalis* is an Ncd-type kinesin-14 motor that uniquely exhibits minus-end-directed processivity over μm distances on single microtubules as individual homodimers. We emphasize that, with a run length of ~3.8 μm, GiKIN14a is a much more processive minus-end-directed kinesin-14 than human kinesin-14 HSET, which only generates minimal processivity of ~80 nm [24]. It is also worth noting that the processive motility of GiKIN14a is distinct from that of another Ncd-type kinesin-14 KIpA, as the latter exhibits processive motility on single microtubules as a homodimer with plus-end directionality [16]. How is GiKIN14a able to achieve minus-end-directed processivity over μm distances on single microtubules as a homodimer? Based on the finding that GiKIN14a contains a microtubule-binding tail (Figures S1A and S1B) and a break in its coiled-coil central stalk (Figure 1B), we speculate that the central stalk of GiKIN14a naturally possesses suitable mechanical flexibility for the N-terminal tail to bind to the same microtubule as the C-terminal motor domains and effectively act as a microtubule tether that enhances processivity. This model is consistent with our previous finding that nonprocessive Ncd, which is predicted to have a continuous coiled-coil stalk, can be made processive by inserting a flexible polypeptide linker that makes the central stalk more flexible [3]. We further found that in addition to acting as a diffusive tether to enable GiKIN14a for long distance minus-end-directed processivity, the N-terminal tail of GiKIN14a also acts to accelerate the stepping and ATP hydrolysis rates of the C-terminal motor domains (Figures 3E and 3F). To our knowledge, GiKIN14a is the first kinesin of any type to have a nonmotor microtubule-binding tail that exerts dual regulatory effects (enabling long distance processivity and enhancing the stepping and ATP hydrolysis rates) on kinesin motility. Thus, the present study not only strengthens the notion that the central stalk is a key determinant of kinesin-14 motility [3] but also markedly expands the diversity of kinesin-14s [8–12,16]. It is important to caution that, as many nonprocessive N-terminal kinesins have discontinuous coiled-coils in the central stalk, having a hinge in the central stalk is not a universally applicable determining factor for the processivity of kinesins from all subfamilies.

How does the N-terminal tail in full-length GiKIN14a act to accelerate the stepping and ATP hydrolysis rates of the C-terminal motor domains? In principle, the N-terminal tail in GiKIN14a could achieve these acceleratory effects by directly interacting with the C-terminal motor domains. We do not favor this idea, however, as we were not able to detect apparent direct motor-tail interaction by analytical size-exclusion chromatography (Figure S1D). Furthermore, a mechanism that depends on the direct motor-tail interaction is incompatible with our observation that increasing the flexibility of the central stalk (which is expected to enhance the ability of the tail to interact with the motor domains) decreases the ATPase rate to nearly the same degree as removing the tail domain entirely (Figure 3F). Previous work by Yildiz and colleagues [28] showed that kinesin-1 mutants engineered to have more flexible neck linkers and less intramolecular tension move significantly slower than their wildtype counterpart, and that their velocities can be restored to nearly normal levels by applying an assisting load via an optical trap. To explain these observations, the authors proposed a model whereby intramolecular tension acts to facilitate the release of the rear motor domain and thus plays an important role in kinesin motility [28]. Inspired by this model, we propose that binding of the N-terminal tail to the same microtubule as the C-terminal motor domains causes full-length GiKIN14a to adopt a stressed *cis* configuration, which induces intramolecular mechanical strain on the neck that accelerates the motor activity of GiKIN14a. This model can account for our finding that increasing the flexibility of the central stalk by inserting a flexible polypeptide linker caused the ATP turnover rate of full-length GiKIN14a to reduce to nearly the same level of the tailless construct GFP-GiKIN14a-Δtail.

Several cytoskeletal motor proteins, such as myosin-V, kinesin-1 and cytoplasmic dynein, are known to move processively by taking either highly coordinated [29,30] or partially coordinated steps [31,32] along their respective cytoskeletal tracks. How does GiKIN14a move on single microtubules to achieve processive motility? Our results showed that while the N-terminal microtubule-binding tail is required for full-length GiKIN14a to achieve processive motility over μm distances (Figures 1E, 1F and 2D), the motor domains and the central stalk alone are sufficient to achieve sub-μm processivity (Figures 3A and S3B). While our results for GiKIN14a-Δtail (Figures 3B and 3E) seem to suggest that GiKIN14a-Δtail moves on the microtubule via a hand-over-hand mechanism [30], additional experiments need to be conducted in the future to uncover the fundamental stepping mechanism underlying the processive motility of GiKIN14a-Δtail. Unlike the nanoparticle tracking experiments for GiKIN14a-Δtail, occasional large jumps were also observed in the tracking experiments for full-length GiKIN14a (black arrows, Figure 3C). Given that we labeled the N-terminal tail of full-length GiKIN14a with a gold nanoparticle for the tracking experiments, these large jumps are likely caused by diffusion of the tail or by diffusion of the tail coupled with stepping of the motor.

At present, it is unclear what physiological role(s) GiKIN14a plays *in vivo.* In most eukaryotic cells, cytoplasmic dynein is the principal motor protein for nearly all intracellular processes that require microtubule minus-end-directed activities [33]. It is also well established that cytoplasmic dynein depends on the dynactin adapter for almost all of its *in vivo* functions [34]. However, both cytoplasmic dynein and dynactin are absent in *G. intestinalis* [35,36], which implies that *G. intestinalis* may have evolved to use kinesin-14

motors to compensate for the loss of cytoplasmic dynein. Dissecting the physiological role(s) of GiKIN14a and the implication of its processivity will be an important subject for future studies.

STAR METHODS

RESOURCE AVAILABILITY

Lead Contact—Further information and requests for resources and reagents should be directed to and will be fulfilled by the Lead Contact, Weihong Qiu (weihong.qiu@physics.oregonstate.edu).

Materials Availability—This study did not generate new unique reagents.

Data and Code Availability—The data of this work and related MATLAB code used for data analysis are available from the corresponding author upon requests.

EXPERIMENTAL MODEL AND SUBJECT DETAILS

METHOD DETAILS

Molecular cloning and protein biochemistry—cDNA of full-length GiKIN14a was codon-optimized for protein expression in the bacterium *E. coli,* commercially synthesized (IDT), and cloned into a modified pET17b vector containing 6xHis-tag and GFP at the N-terminus via Gibson assembly (NEB). Full-length GFP-GiKIN14a was confirmed by DNA sequencing (GeneScript). cDNAs of other GiKIN14a constructs (GFP-GiKIN14a-Δtail, GFP-GiKIN14a-tail, GFP-GiKIN14a-Δtail^{T}, and GiKIN14a-stalk that contains residues 130–224 of GiKIN14a) were all derived from GFP-GiKIN14a using the Q5 site-directed mutagenesis kit (NEB) and confirmed by DNA sequencing (GeneScript). cDNAs of two Ncd stalk constructs, Ncd-WT-stalk that contains residues 196–348 of Ncd and Ncd-3xGS-stalk that contains residues 196–348 of Ncd and an insertion of a polypeptide linker (-GSGSGS-) after T271, were derived from cDNA of full-length Ncd using the Q5 site-directed mutagenesis kit (NEB) and confirmed by DNA sequencing (GeneScript).

For protein expression, a plasmid containing the desired construct was transformed into the BL21 Rosetta (DE3) competent cells (Novagen). Cells were grown at 37 °C in TPM (containing 20 g tryptone, 15 g yeast extract, 8 g NaCl, 2 g Na_2HPO_4, and 1 g KH_2PO_4 per 1 liter) supplemented with 50 μg ml^{-1} ampicillin and 30 μg ml^{-1} chloramphenicol. Expression was induced by cold shock on ice at OD = 0.8–1 with 0.1 mM IPTG, and incubation was continued for an additional 12–14 hours at 18 °C. Cell pellets were harvested by centrifugation at 5500 x g for 10 minutes using a S-5.1 rotor (Beckman Coulter), and stored at −80 °C prior to cell lysis. For protein purification, cell pellets were re-suspended in the lysis buffer [50 mM sodium phosphate buffer (pH 7.2) containing 250 mM NaCl, 1 mM $MgCl_2$, 0.5 mM ATP, 10 mM β-mercaptoethanol, 20 mM imidazole and protease inhibitor cocktail] and lysed via sonication (Branson Sonifier 450). The cell lysate was then centrifuged at 21,000 x g for 30 minutes using a 75 Ti rotor (Beckman Coulter). The supernatant was incubated with TALON metal affinity resin (Takarabio) by end-to-end mixing at 4 °C for 1 hour. The protein/beads slurry was then applied to a Poly-Prep column

(Bio-Rad) and washed twice with 10 column volumes of the wash buffer [50 mM sodium phosphate buffer (pH 7.2) containing 250 mM NaCl, 1 mM $MgCl_2$, 0.1 mM ATP, 10 mM β-mercaptoethanol, 20 mM imidazole and protease inhibitor cocktail]. The protein was eluted with 5 column volumes of the elution buffer (50 mM sodium phosphate buffer, pH 7.2, 250 mM NaCl, 1 mM $MgCl_2$, 0.5 mM ATP, 10 mM β-mercaptoethanol, 250 mM imidazole, and 5% glycerol), flash frozen in liquid nitrogen, and stored at −80 °C prior to usage.

Microtubule preparation—Taxol-stabilized polarity-marked microtubules with bright plus-ends for the single-molecule motility assay were prepared as previously described [16]. Briefly, a dim tubulin mix containing 17 μM unlabeled tubulin, 0.8 μM HiLyte 647-tubulin and 17 μM biotinylated tubulin was first incubated in BRB80 with 0.5 mM GMPCPP (Jena Bioscience) at 37 °C for at least 2 hours to make dim microtubules. The polymerized dim microtubules were pelleted by centrifuging at 250.0 x g for 7 minutes at 37 °C in a TLA100 rotor (Beckman Coulter). The pellet was re-suspended in a bright tubulin mix containing 7.5 μM unlabeled tubulin, 4 μM HiLyte 647-tubulin, and 15 μM NEM-tubulin in BRB80 with 2 mM GMPCPP and incubated at 37 °C for 30 minutes to cap the plus-end of the dim microtubules. The polarity-marked microtubules were pelleted at 20.0 x g for 7 minutes at 37 °C in the TLA100 rotor (Beckman Coulter), and finally resuspended in BRB80 with 40 μM taxol. The method to make polarity-marked microtubule for microtubule gliding assay is similar except the dim tubulin mix was without biotinylated tubulin and the HiLyte 647-labeled tubulin is replaced with tetramethylrhodamine (TMR)-labeled tubulin in both the dim and bright tubulin mix.

For making microtubules lacking the C-terminal E-hooks, taxol-stabilized microtubules were similarly prepared from unlabeled tubulin (200 μM) using the aforementioned protocol, subsequently centrifuged at 100,000 x g using a TLA100 rotor (Beckman Coulter) for 20 minutes at 37 °C, and then resuspended in a warm (37 °C), 1/0.8 (v/v) PME-glycerol buffer. To proteolytically cleave the E-hooks from microtubules, the microtubule resuspension was incubated with 275 μg ml^{-1} freshly prepared subtilisin at 37 °C for 60 minutes, and the cleavage reaction was terminated by adding 1 mM PMSF (freshly dissolved in DMSO). After the digestion reaction, microtubules were pelleted by centrifugation at 100,000 x g using a TLA100 rotor (Beckman Coulter) for 20 minutes at 37 °C, and the resulting microtubule pellet was carefully resuspended with a warm (37 °C) BRB80 buffer supplemented with 200 μM taxol and stored at 37°C for further use. SDS-PAGE was used to confirm the completion of subtilisin digestion of the E-hooks.

Microtubule co-sedimentation assays—For the microtubule co-sedimentation experiments, purified GFP-GiKIN14a-tail was mixed with regular or subtilisin-digested microtubules (in BRB50 supplemented with 40 μM taxol; final [tubulin] = 20 μM), subsequently incubated at room temperature for 30 minutes, and then centrifuged at 100,000 x g using a TLA100 rotor (Beckman Coulter) for 15 minutes at 37 °C. SDS-GAGE was used to analyze the amount of protein in the pellet and supernatant. Because GFP-GiKIN14a-tail (Molecular Weight = ~52 kDa) and the α-tubulin monomer (Molecular Weight = ~55k Da) were nearly indistinguishable in the standard Coomassie-stained SDS-PAGE, GFP-

GiKIN14a-tail in SDS-PAGE was unstained and instead detected through GFP fluorescence via UV illumination.

Analytical size-exclusion chromatography—For analytical size-exclusion chromatography (SEC) of GFP-GiKIN14a-Δtail or GFP-GiKIN14a-tail, 500 μL of purified protein was applied to a Superdex 200 Increase 10/300 GL column (GE Life Sciences) that was pre-equilibrated with BRB50 (50 mM PIPES, pH 6.8, 1 mM EGTA and 1 mM $MgCl_2$) supplemented with 50 mM KCl. Elution fractions of 800 μl were collected and subsequently analyzed using standard SDS-PAGE. The procedure of analytical SEC for the protein mixture containing both GFP-GiKIN14a-Δtail and GFP-GiKIN14a-tail was nearly identical to that of GFP-GiKIN14a-Δtail or GFP-GiKIN14a-tail, except that the protein mix was incubated on ice for 1 hour before being applied to the column.

Circular dichroism (CD) spectroscopy—All CD experiments were performed at 25 °C using a JASCO J-815 spectropolarimeter and a quartz cuvette with a path length of 0.1 cm. Coiled-coil domains of kinesin-14s were dialyzed into 10 mM phosphate buffer, and data was taken within 24 hours of purification. CD was measured at a concentration of peptide between 45 and 70 μM, determined by Bradford assay. Samples were shown to be free of disulfide-induced aggregation by SDS-PAGE under nonreducing conditions. Data are expressed as mean residue molar ellipticity.

Total internal reflection fluorescence (TIRF) microscopy—All TIRF microscopy experiments were performed at room temperature using the Axio Observer Z1 objective-type TIRF microscope (Zeiss) equipped with a 100× 1.46 NA oil-immersion objective and a back-thinned electron multiplier CCD camera (Photometrics). Flow chambers were made by attaching a coverslip to a microscope glass slide by a double-sided tape. Except for the ensemble microtubule-gliding experiments, all experiments used coverslips functionalized with Biotin-PEG to reduce the nonspecific surface absorption of protein molecules.

For the microtubule-gliding assay, GFP-GiKIN14a and GFP-GiKIN14a-Δtail were immobilized on the glass surface using the anti-HIS tag antibody (Thermo Fisher Scientific). After washing away unbound motor proteins with BRB50 supplemented with 20 μM taxol and 1.3 mg ml^{-1} casein, polarity-marked TMR-labeled microtubules were to the flow chamber. The motility buffer (BRB50 containing 1 mM ATP, 10 mM KCl, 25 μM taxol, 1.3 mg ml^{-1} casein and an oxygen scavenger system [16] was then added into the flow chamber after washing away unbound microtubules. Time-lapse images were taken at 1 frame per 5 seconds for 5 minutes.

For the single-molecule motility experiments of GFP-GiKIN14a, polarity-marked HiLyte 647/Biotin-labeled microtubules were immobilized on the biotin-PEG-functionalized coverslips through the biotin-streptavidin-biotin interaction. After washing away unbound microtubules with BRB50 supplemented with 20 μM taxol and 1.3 mg ml^{-1} casein, GFP-GiKIN14a molecules diluted in the motility buffer (BRB50 supplemented with 1 mM ATP, 10 mM KCl, 25 μM taxol, 1.3 mg ml^{-1} casein, and an oxygen scavenger system [16] were added into the flow chamber. Time-lapse images were recorded with the exposure time of 100 ms at 1 frame per second for 10 minutes. For the single-molecule experiments of GFP-

GiKIN14a-Δtail, the experimental procedure was nearly the same as that of GFP-GiKIN14a except that the time-lapse images were recorded for a total duration of 5 minutes at 5 frames per second. For the single-molecule experiments of GFP-GiKIN14a-tail, the motility buffer did not contain ATP.

For the single-molecule photobleaching assay, HiLyte 647/Biotin-labeled microtubules were immobilized on the functionalized coverslips similarly to the single-molecule motility assay. Motor proteins diluted in the motility buffer that lacked both ATP and the oxygen scavenger system were added on the microtubules. After washing away unbound motor proteins, time-lapse image sequences were continuously recorded with an exposure time of 200 ms until the field of view was completely bleached of fluorescence signal. Photobleaching steps of individual kinesin motors were obtained by measuring the fluorescence intensity in ImageJ (NIH).

Dark-field gold nanoparticle tracking—A biotin-streptavidin approach was used to attach 30-nm gold nanoparticles (BBI Solutions) to the GiKIN14a motors. For full-length GiKIN14a, the gold nanoparticle was attached via the N-terminal GFP. A SNAP-tagged GFP-binding protein (GBP) was expressed in *E. coli* and purified by affinity chromatography. A biotinylated 20 base-pair double-strand oligonucleotide (IDT) was then bound to the SNAP tag using BG-GLA-NHS (New England Biolabs). Biotin-DNA-GBP was then mixed with GFP-GiKIN14a at ~1:1 ratio, and this solution was then mixed with streptavidin- gold at 1:2.5 or 1:12.5 (total motor: gold). For the GFP-GiKIN14a-Δtail construct, an Avi-tag was fused to the N-terminus immediately after the His-tag and co-expressed with bacterial biotin ligase as done previously [25]. Biotinylated protein concentration was measured using a fluorescence biotin quantification kit (Thermo Fisher Scientific), and streptavidin-coated gold nanoparticles were mixed with biotinylated-motors at a stoichiometric excess (typically 1:0.7 gold:biotin motor or lower). For both motors, mixing was done in BRB50 plus 0.5 mg ml^{-1} casein and 2 mM ATP for 30 minutes on ice. Gold nanoparticles were then pelleted at 20,000 x g for 4 minutes and resuspended at working concentration levels (~300 pM) in the imaging solution: 0.5 mg ml^{-1} casein, 10 μM taxol, 20 mM glucose, 20 μg ml^{-1} glucose oxidase, 8 μg ml^{-1} catalase, 0.2 mg ml^{-1} BSA, 1:200 β-mercaptoethanol, and 2 mM MgATP in BRB50 (50 mM K-PIPES, 1 mM EGTA, 1 mM $MgCl_2$, pH 6.8). Dark-field nanoparticle tracking experiments were carried out as previously described [25]. All experiments were performed at 22–23 °C. Gold nanoparticles were imaged at 1,000 frames per second using a custom-built total internal reflection dark-field microscope as described previously [25].

Landing rate assay—The gold landing rate assay was performed by first pre-incubating a number of molar ratios of biotinylated motors to streptavidin-labeled 30-nm gold nanoparticles on ice for 30 minutes and then imaging in the total internal reflection dark-field microscope. Images were acquired at 10 frames per second. Rhodamine-labeled microtubules were visualized through a 570-nm long-pass filter (Thorlabs). A landing event was quantified as any time a gold nanoparticle landed on a microtubule and moved a detectable distance (the shortest measured distance was ~40 nm).

Microtubule-stimulated ATPase assay—The microtubule-stimulated ATPase assay was done using an enzyme-coupled system with NADH as a reporter for ATP, as described previously [37]. Observed NADH depletion rates were normalized by the total motor dimer concentration to obtain the ATP turnover rate. Motor concentration was measured by fluorescent nucleotide exchange as described previously [37]. For GFP-GiKIN14a-Δtail, 40 nM motor was used, and NADH concentration was monitored by absorbance at 350 nm using an Agilent 9453A UV-vis spectrophotometer. For full-length GFP-GiKIN14a, 25 nM motor was used, but microtubule crosslinking confounded absorbance signals, so NADH concentration was instead monitored by fluorescence using a Shimadzu 3000 spectrofluorometer. NADH was excited at 350 nm and emission was measured at 460 nm. Fluorescence intensity was converted to concentration using a calibration curve generated by adding known amounts of ADP to the reporter system.

QUANTIFICATION AND STATISTICAL ANALYSIS

Analysis of single-molecule motility experiments—Kymographs from the single-molecule motility experiments were generated and analyzed in ImageJ (NIH) for extracting the velocity and run-length information of individual motors. Only kymograph lines having at least 4 pixels in both X- and Y-directions were included in the analysis. Velocity and run-length histograms were fitted using MATLAB (MathWorks).

Analysis of dark-field gold nanoparticle tracking—Movies from dark-field gold nanoparticle tracking experiments were analyzed to obtain (X, Y, t) data by fitting moving dots with point-spread functions using FIESTA [38]. Coordinate data (X, Y) were rotated to find position along the microtubule [25], which was then analyzed with a step-finding algorithm [39]. Step size histograms and dwell time distributions were all fitted using MATLAB (MathWorks).

Supplementary Material

Refer to Web version on PubMed Central for supplementary material.

ACKNOWLEDGEMENTS

This work was supported in part by the National Science Foundation (MCB-1616462 to W.Q. and MCB-1617019 to E.J.B.), the National Institutes of Health (GM127922 to W. Q. and GM076476 to W.O.H.), and the National Cancer Institute (F99CA223018 to K.J.M.).

References

1. She Z-Y, and Yang W-X (2017). Molecular mechanisms of kinesin-14 motors in spindle assembly and chromosome segregation. J. Cell Sci. 130, 2097–2110. [PubMed: 28668932]
2. Adam RD (2001). Biology of Giardia lamblia. Clin. Microbiol. Rev. 14, 447–475. [PubMed: 11432808]
3. Wang P, Tseng K-F, Gao Y, Cianfrocco M, Guo L, and Qiu W (2018). The central stalk determines the motility of mitotic kinesin-14 homodimers. Curr. Biol. 28, 2302–2308.e3. [PubMed: 30017487]
4. Drummond DR (2011). Regulation of microtubule dynamics by kinesins. Semin. Cell Dev. Biol. 22, 927–934. [PubMed: 22001250]
5. Vale RD (2003). The molecular motor toolbox for intracellular transport. Cell 112, 467–480. [PubMed: 12600311]

6. Lawrence CJ, Dawe RK, Christie KR, Cleveland DW, Dawson SC, Endow SA, Goldstein LSB, Goodson HV, Hirokawa N, Howard J, et al. (2004). A standardized kinesin nomenclature. J. Cell Biol. 167, 19–22. [PubMed: 15479732]
7. Hirokawa N, Noda Y, Tanaka Y, and Niwa S (2009). Kinesin superfamily motor proteins and intracellular transport. Nat. Rev. Mol. Cell Biol. 10, 682–696. [PubMed: 19773780]
8. Hepperla AJ, Willey PT, Coombes CE, Schuster BM, Gerami-Nejad M, McClellan M, Mukherjee S, Fox J, Winey M, Odde DJ, et al. (2014). Minus-end-directed kinesin-14 motors align antiparallel microtubules to control metaphase spindle length. Dev. Cell 31, 61–72. [PubMed: 25313961]
9. Mieck C, Molodtsov MI, Drzewicka K, van der Vaart B, Litos G, Schmauss G, Vaziri A, and Westermann S (2015). Non-catalytic motor domains enable processive movement and functional diversification of the kinesin-14 Kar3. eLife 4.
10. Tseng K-F, Wang P, Lee Y-RJ, Bowen J, Gicking AM, Guo L, Liu B, and Qiu W (2018). The preprophase band-associated kinesin-14 OsKCH2 is a processive minus-end-directed microtubule motor. Nat. Commun. 9, 1–11. [PubMed: 29317637]
11. Decarreau J, Wagenbach M, Lynch E, Halpern AR, Vaughan JC, Kollman J, and Wordeman L (2017). The tetrameric kinesin Kif25 suppresses pre-mitotic centrosome separation to establish proper spindle orientation. Nat. Cell Biol. 19, 384–390. [PubMed: 28263957]
12. Hata S, Pastor Peidro A, Panic M, Liu P, Atorino E, Funaya C, Jakle U, Pereira G, and Schiebel E (2019). The balance between KIFC3 and EG5 tetrameric kinesins controls the onset of mitotic spindle assembly. Nat. Cell Biol. 21, 1138–1151. [PubMed: 31481795]
13. McDonald HB, Stewart RJ, and Goldstein LSB (1990). The kinesin-like ncd protein of Drosophila is a minus end-directed microtubule motor. Cell 63, 1159–1165. [PubMed: 2261638]
14. Walker RA, Salmon ED, and Endow SA (1990). The Drosophila claret segregation protein is a minus-end directed motor molecule. Nature 347, 780–782. [PubMed: 2146510]
15. O'Connell MJ, Meluh PB, Rose MD, and Morris NR (1993). Suppression of the bimC4 mitotic spindle defect by deletion of klpA, a gene encoding a KAR3-related kinesin-like protein in Aspergillus nidulans. J. Cell Biol. 120, 153–162. [PubMed: 8416986]
16. Popchock AR, Tseng K-F, Wang P, Karplus PA, Xiang X, and Qiu W (2017). The mitotic kinesin-14 KlpA contains a context-dependent directionality switch. Nat. Commun. 8, 1–9. [PubMed: 28232747]
17. Weinger JS, Qiu M, Yang G, and Kapoor TM (2011). A nonmotor microtubule binding site in kinesin-5 is required for filament crosslinking and sliding. Curr. Biol. 21, 154–160. [PubMed: 21236672]
18. Gudimchuk N, Vitre B, Kim Y, Kiyatkin A, Cleveland DW, Ataullakhanov FI, and Grishchuk EL (2013). Kinetochore kinesin CENP-E is a processive bi-directional tracker of dynamic microtubule tips. Nat. Cell Biol. 15, 1079–1088. [PubMed: 23955301]
19. Stumpff J, Du Y, English CA, Maliga Z, Wagenbach M, Asbury CL, Wordeman L, and Ohi R (2011). A tethering mechanism controls the processivity and kinetochore-microtubule plus-end enrichment of the kinesin-8 Kif18A. Mol. Cell 43, 764–775. [PubMed: 21884977]
20. Su X, Qiu W, Gupta ML, Pereira-Leal JB, Reck-Peterson SL, and Pellman D (2011). Mechanisms underlying the dual-mode regulation of microtubule dynamics by Kip3/kinesin-8. Mol. Cell 43, 751–763. [PubMed: 21884976]
21. Jonsson E, Yamada M, Vale RD, and Goshima G (2015). Clustering of a kinesin-14 motor enables processive retrograde microtubule-based transport in plants. Nat. Plants 1, 1–7.
22. Walter WJ, Machens I, Rafieian F, and Diez S (2015). The non-processive rice kinesin-14 OsKCH1 transports actin filaments along microtubules with two distinct velocities. Nat. Plants 1, 1–5.
23. Furuta K, Furuta A, Toyoshima YY, Amino M, Oiwa K, and Kojima H (2013). Measuring collective transport by defined numbers of processive and nonprocessive kinesin motors. Proc. Natl. Acad. Sci. 110, 501–506. [PubMed: 23267076]
24. Reinemann DN, Norris SR, Ohi R, and Lang MJ (2018). Processive kinesin-14 HSET exhibits directional flexibility depending on motor traffic. Curr. Biol. 28, 2356–2362.e5. [PubMed: 30017484]
25. Mickolajczyk KJ, and Hancock WO (2017). Kinesin processivity is determined by a kinetic race from a vulnerable one-head-bound state. Biophys. J. 112, 2615–2623. [PubMed: 28636917]

26. Leduc C, Ruhnow F, Howard J, and Diez S (2007). Detection of fractional steps in cargo movement by the collective operation of kinesin-1 motors. Proc. Natl. Acad. Sci. U. S. A. 104, 10847–10852. [PubMed: 17569782]
27. Block SM, Goldstein LS, and Schnapp BJ (1990). Bead movement by single kinesin molecules studied with optical tweezers. Nature 348, 348–352. [PubMed: 2174512]
28. Yildiz A, Tomishige M, Gennerich A, and Vale RD (2008). Intramolecular strain coordinates kinesin stepping behavior along microtubules. Cell 134, 1030–1041. [PubMed: 18805095]
29. Yildiz A, Forkey JN, McKinney SA, Ha T, Goldman YE, and Selvin PR (2003). Myosin V walks hand-over-hand: single fluorophore imaging with 1.5-nm localization. Science 300, 2061–2065. [PubMed: 12791999]
30. Yildiz A, Tomishige M, Vale RD, and Selvin PR (2004). Kinesin walks hand-over-hand. Science 303, 676–678. [PubMed: 14684828]
31. DeWitt MA, Chang AY, Combs PA, and Yildiz A (2012). Cytoplasmic dynein moves through uncoordinated stepping of the AAA+ ring domains. Science 335, 221–225. [PubMed: 22157083]
32. Qiu W, Derr ND, Goodman BS, Villa E, Wu D, Shih W, and Reck-Peterson SL (2012). Dynein achieves processive motion using both stochastic and coordinated stepping. Nat. Struct. Mol. Biol. 19, 193–200. [PubMed: 22231401]
33. Roberts AJ, Kon T, Knight PJ, Sutoh K, and Burgess SA (2013). Functions and mechanics of dynein motor proteins. Nat. Rev. Mol. Cell Biol. 14, 713–726. [PubMed: 24064538]
34. Reck-Peterson SL, Redwine WB, Vale RD, and Carter AP (2018). The cytoplasmic dynein transport machinery and its many cargoes. Nat. Rev. Mol. Cell Biol. 19, 382–398. [PubMed: 29662141]
35. Hammesfahr B, and Kollmar M (2012). Evolution of the eukaryotic dynactin complex, the activator of cytoplasmic dynein. BMC Evol. Biol. 12, 95. [PubMed: 22726940]
36. Morrison HG, McArthur AG, Gillin FD, Aley SB, Adam RD, Olsen GJ, Best AA, Cande WZ, Chen F, Cipriano MJ, et al. (2007). Genomic minimalism in the early diverging intestinal parasite Giardia lamblia. Science 317, 1921–1926. [PubMed: 17901334]
37. Chen G-Y, Arginteanu DFJ, and Hancock WO (2015). Processivity of the kinesin-2 KIF3A results from rear head gating and not front head gating. J. Biol. Chem. 290, 10274–10294. [PubMed: 25657001]
38. Ruhnow F, Zwicker D, and Diez S (2011). Tracking single particles and elongated filaments with nanometer precision. Biophys. J. 100, 2820–2828. [PubMed: 21641328]
39. Kerssemakers JWJ, Munteanu EL, Laan L, Noetzel TL, Janson ME, and Dogterom M (2006). Assembly dynamics of microtubules at molecular resolution. Nature 442, 709–712. [PubMed: 16799566]

Highlights

- GiKIN14a without the N-terminal microtubule-binding tail is minimally processive
- The N-terminal tail enables full-length GiKIN14a for long-distance processivity
- GiKIN14a moves on the microtubule by taking discrete steps
- The N-terminal tail accelerates the stepping and ATP hydrolysis rates of GiKIN14a

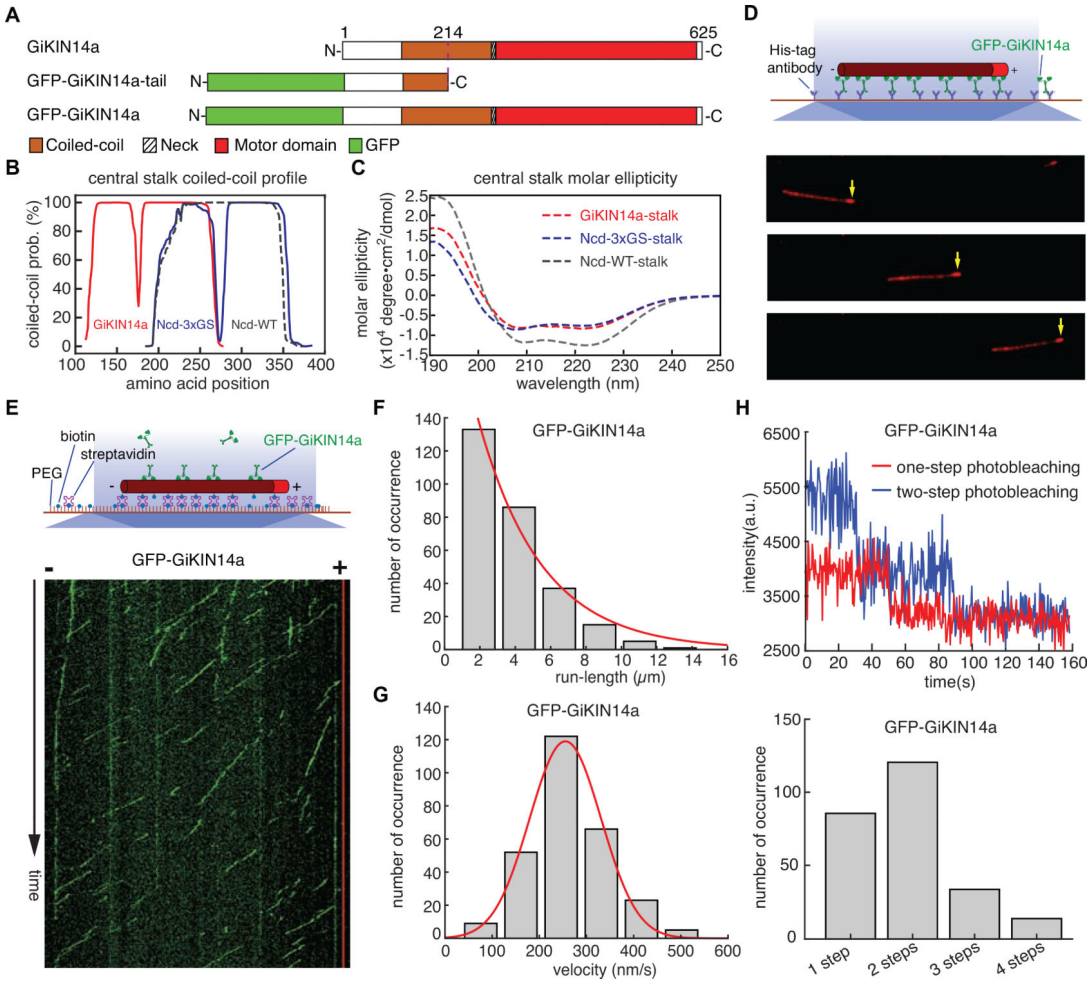

Figure 1. Full-Length GiKIN14a Exhibits Minus-End-Directed Processivity over Micrometer Distances on Single Microtubules as Individual Homodimers.

(A) Schematic diagrams of full-length GiKIN14a, GFP-GiKIN14a-tail, and GFP-GiKIN14a.

(B) Predicted coiled-coil profiles of the central stalks of GiKIN14a (red), Ncd-3xGS (blue), and Ncd-WT (dark grey).

(C) Circular dichroism spectra of three central stalk constructs, GiKIN14a-stalk (red), Ncd-3xGS-stalk (blue), and Ncd-WT-stalk (dark grey). GiKIN14a-stalk contains residues 130–224 of GiKIN14a, Ncd-WT-stalk contains residues 196–348 of Ncd, and Ncd-3xGS-stalk contains residues 196–348 of Ncd and an insertion of a polypeptide linker (-GSGSGS-) after T271.

(D) Microtubule gliding by immobilized GFP-GiKIN14a molecules. Top: Schematic of the microtubule-gliding assay. Bottom: Micrograph montage showing that surface-immobilized GFP-GiKIN14a molecules glide microtubules with minus-end-directed motility. Yellow arrows indicate the plus ends of polarity-marked microtubules. Scale bar: 5 μm (horizontal).

(E) Single-molecule motility of GFP-GiKIN14a on immobilized microtubules. Top: Schematic diagram of the single-molecule motility assay on polarity-marked single microtubules. Bottom: Example kymograph of individual GFP-GiKIN14a molecules

exhibiting processive minus-end-directed motility on single microtubules. Scale bars: 1 minute (vertical), and 5 μm (horizontal).

(F) Run-length histogram of GFP-GiKIN14a. Red line indicates a single-exponential decay fit.

(G) Velocity histogram of GFP-GiKIN14a. Red line indicates a Gaussian fit.

(H) Photobleaching analysis of GFP-GiKIN14a. Top: Example fluorescence intensity traces of individual GFP-GiKIN14a molecules. Bottom: Histogram of the photobleaching steps of GFP-GiKIN14a (n = 255).

See also Figures S1 and S2, and Video S1.

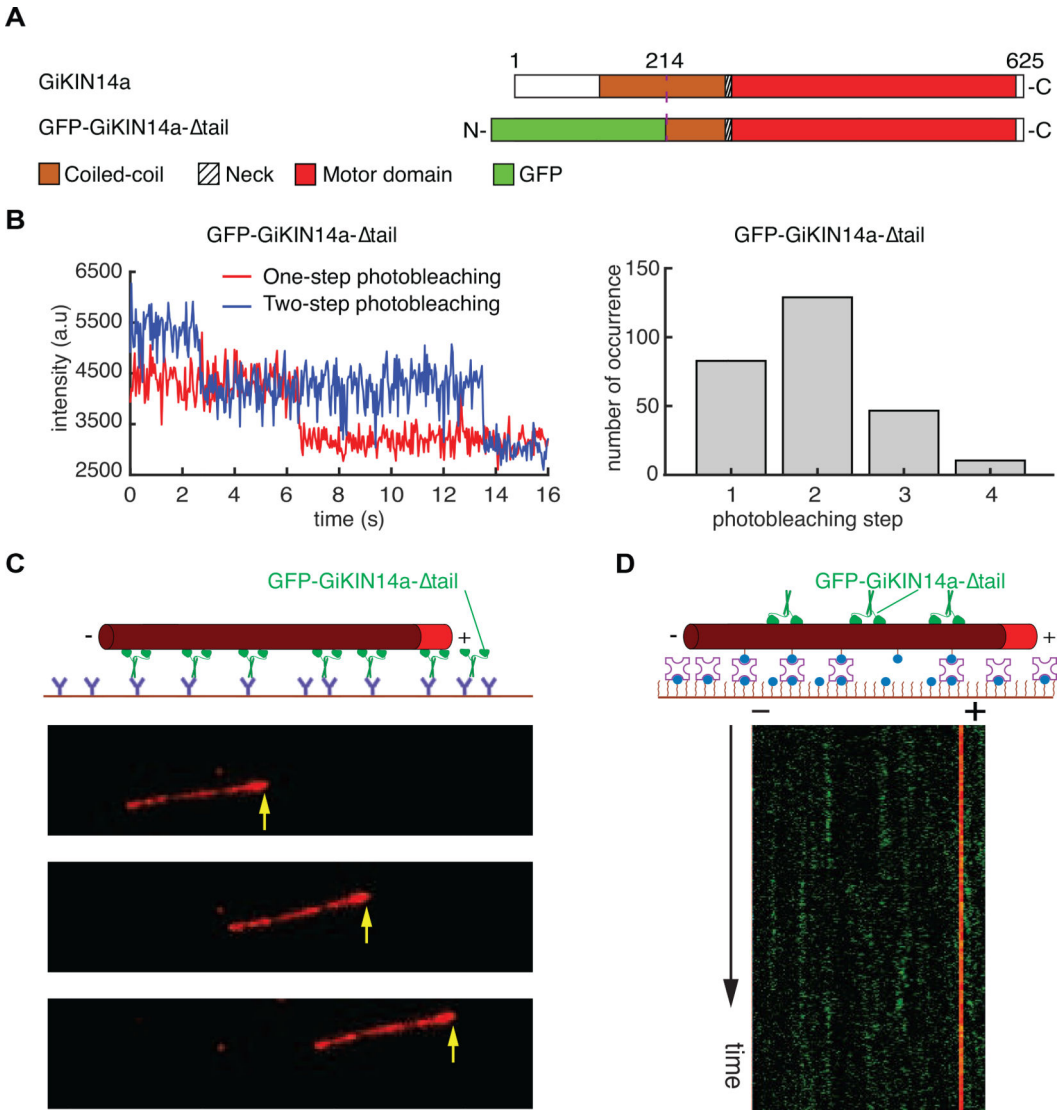

Figure 2. GiKIN14a Depends on Its N-terminal Microtubule-Binding Tail to Achieve Micrometer-Distance Processivity.

(A) Schematic diagrams of full-length GiKIN14a and GFP-GiKIN14a-Δtail.

(B) Photobleaching analysis of GFP-GiKIN14a-Δtail. Left: Example fluorescence intensity traces over time of individual GFP-GiKIN14a-Δtail molecules on microtubules. Right: Histogram of the photobleaching steps of GFP-GiKIN14a-Δtail (n = 270).

(C) Micrograph montage showing that GFP-GiKIN14a-Δtail causes a polarity-marked microtubule to glide with its plus end leading. Yellow arrows indicate the microtubule plus ends. Scale bar: 5 μm (horizontal).

(D) Example kymograph showing that GFP-GiKIN14a-Δtail (green) fails to exhibit pm-distance processivity on single microtubules (red). The thin red vertical line on the right indicates the brightly labeled microtubule plus end. Scale bars: 30 seconds (vertical), and 5 μm (horizontal).

See also Figures S1 and S2, and Video S2.

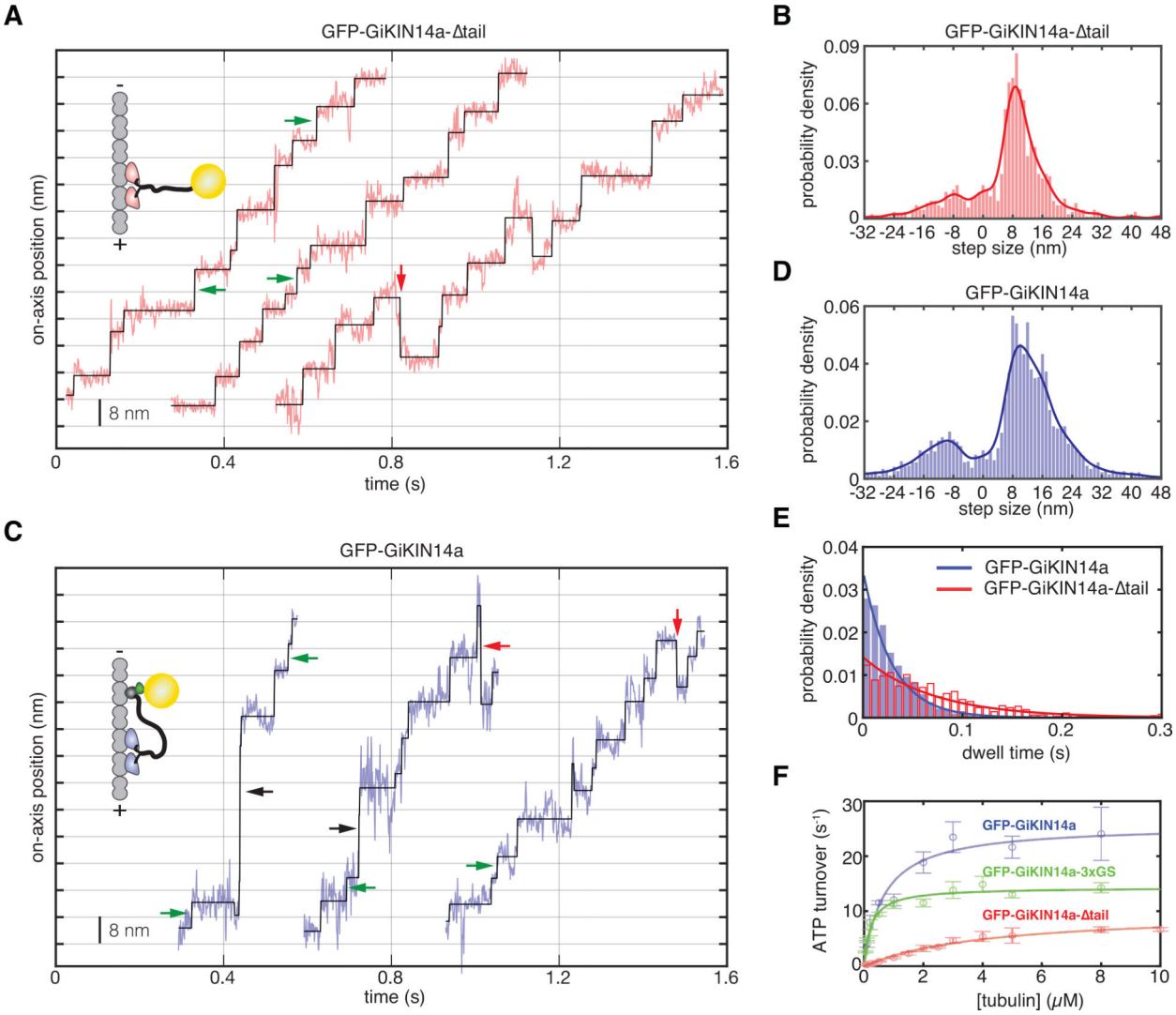

Figure 3. The N-terminal Tail Enables GiKIN14a to Exhibit Enhanced Stepping and ATP Hydrolysis Rates.

(A) Example dark-field tracking traces for GFP-GiKIN14a-Δtail with a gold nanoparticle attached at the N-terminus.

(B) Step size distribution for the GFP-GiKIN14a-Δtail (n = 861 steps from 27 molecules, 5 slides). Solid line is the kernel density curve with peaks at 8.7 and −7.8 nm.

(C) Example dark-field tracking traces for full-length GFP-GiKIN14a with a gold nanoparticle at the N-terminus.

(D) Step size distribution for full-length GFP-GiKIN14a (n = 2,653 steps from 35 molecules, 8 slides). Solid line is the kernel density curve with peaks at 10.0 and −9.5 nm.

(E) Dwell time distributions for the steps of GFP-GiKIN14a-Δtail (red) and full-length GFP-GiKIN14a (blue). Red and blue lines each indicate a single exponential decay fit.

(F) Microtubule-stimulated ATPase analysis of GFP-GiKIN14a-Δtail (red), GFP-GiKIN14a-3xGS (green) and full-length GFP-GiKIN14a (blue). All data points represent at least five measurements, and are shown as mean ± SEM.

See also Figure S3 and Video S3.

KEY RESOURCES TABLE

REAGENT or RESOURCE	SOURCE	IDENTIFIER
Antibodies		
Anti-HIS tag antibody	Thermo Fisher Scientific	Cat# MA1-135-HRP
Recombinant DNA		
Plasmid: GFP-GiKIN14a	This manuscript	N/A
Plasmid: GFP-GiKIN14a-Δtail	This manuscript	N/A
Plasmid: GFP-GiKIN14a-tail	This manuscript	N/A
Plasmid: GFP-GiKIN14a-Δtail^{T}	This manuscript	N/A
Plasmid: GiKIN14a-stalk	This manuscript	N/A
Plasmid: Ncd-WT-stalk	This manuscript	N/A
Plasmid: Ncd-3xGS-stalk	This manuscript	N/A
cDNA of full-length GiKIN14a	IDT	N/A
cDNA of full-length Ncd	IDT	N/A
Bacterial and Virus Strains		
MAX Efficiency™ DH5α Competent Cells	Thermo Fisher Scientific	Cat# 18258012
Rosetta™(DE3) Competent Cells	Novagen	Cat# 70954
Chemicals, Peptides, and Recombinant Proteins		
Tryptone	Fisher Scientific	Cat# BP1421-500
Yeast Extract	Sigma-Aldrich	Cat# Y1625
Sodium chloride	Strem Chemicals	Cat# 11-1100
Sodium phosphate monobasic monohydrate	Sigma-Aldrich	Cat# S9638
Potassium phosphate monobasic	Sigma-Aldrich	Cat# P5655
Ampicillin sodium salt USP	VWR	Cat# 97061-442
Chloramphenicol	Thermo Fisher Scientific	Cat# BP904-100
IPTG	Thermo Fisher Scientific	Cat# 15529019
Sodium phosphate monobasic monohydrate	Sigma-Aldrich	Cat# S9638
Magnesium chloride hexahydrate ACS	VWR	Cat# 97061-354
β-mercaptoethanol	Sigma-Aldrich	Cat# M6250
Imidazole	Sigma-Aldrich	Cat# I5513
GMPCPP	Jena Bioscience	Cat# NU-405L
HiLyte 647-tubulin	Cytoskeleton	Cat# TL670M-B
Tubulin: Porcine brain	This paper	N/A
Biotinylated tubulin: Porcine brain	This paper	N/A
Taxol	Sigma-Aldrich	Cat# PHL89806
Subtilisin	Sigma-Aldrich	Cat# P8038
DMSO	Thermo Fisher Scientific	Cat# BP231-100
PMSF Protease Inhibitor	Thermo Fisher Scientific	Cat# 36978
PIPES disodium salt	Thermo Fisher Scientific	Cat# AC215092500

REAGENT or RESOURCE	SOURCE	IDENTIFIER
Gold nanoparticles 30nm	BBI Solutions	SKU# EM.GC30
BG-GLA-NHS	New England Biolabs	Cat# S9151S
Critical Commercial Assays		
Branson Ultrasonics™ Sonifier	Thermo Fisher Scientific	Cat# 22-309783
TALON Metal Affinity Resin	Takarabio	Cat# 635606
Poly-Prep column	Bio-Rad	Cat# 7311550
Superdex 200 Increase 10/300 GL column	GE Life Sciences	Cat# 28990944
Spectropolarimeter J-815	JASCO	N/A
Quick Start™ Bradford Protein Assay Kit 1	Bio-Rad	Cat# 5000201
Axio Observer Z1 objective-type TIRF microscope	Zeiss	N/A
Pierce™ Fluorescence Biotin Quantitation Kit	Thermo Fisher Scientific	Cat# 46610
FGL570 - Ø25 mm OG570 Colored Glass Filter, 570 nm Longpass	Thorlabs	Cat# FGL570
Gibson Assembly® Master Mix	New England Biolabs	Cat# E2611L
Q5® Site-Directed Mutagenesis Kit	New England Biolabs	Cat# E0554S
Software and Algorithms		
FIESTA	FIESTA	https://fusionforge.zih.tu-dresden.de/plugins/mediawiki/wiki/fiesta/index.php/FIESTA
ImageJ	NIH	https://imagej.nih.gov/ij/
MATLAB	MathWorks	https://www.mathworks.com/products/matlab.html